A Product Distribution Paradox on Scaling Up a Stirred Batch Reactor

R. Mann and A. M. El-Hamouz
Dept. of Chemical Engineering, UMIST, Manchester M60 1QD, England

For a triplet competitive-consecutive halogenation sequence forming mono-, di- and trihalogenated products of the form, $A + B \rightarrow R + B \rightarrow S + B \rightarrow T$, under semibatch operation adding B to A, if perfect mixing could be assumed at all scales, the product distribution would be unchanged on scaling up. However, if the reaction rates are reasonably faster than the mixing rate, the semibatch addition of B to A will be imperfectly backmixed, exhibiting macroscale concentration gradients. This partial segregation of the primary reagents is capable of modifying the selectivity and corresponding appearance of R, S and T in the course of the batch. Imperfect mixing is quantified using the networks-of-zones model. The effect of scaling up at equal tip speed is examined for a lab-scale 0.3-dm^3 reactor, a semitech 30-dm^3 reactor, and a production-scale 3,000-dm^3 vessel. The intensity of partial segregation is weak at the lab scale, but very severe at the production scale. The lab-scale reactor is therefore close to perfectly backmixed, and the primary, secondary and tertiary products appear in sequence. At the semitech scale the increased partial segregation causes the final product to initially precede the secondary product paradoxically but lag the initial product. At the large scale the more severe segregation between A and B gives an even greater paradox, whereby the final product appears ahead of both the primary and secondary ones. The segregated concentration fields of A and B are visualized as sectional image reconstructions for networks comprising on the order of 1,000 zones. Localized intensive plumes of B emanating from the addition point cause the paradoxical reversals of product sequences. The calculations are directly relevant to real industrial miscible liquid halogenations for which product distribution paradoxes have been observed (Haywood, 1990).

Introduction

Perfect mixing is often assumed in the assessment and description of stirred-vessel chemical reactors. It is frequently the case, however, that the assumption remains untested. In practice, the validity of assumed perfect mixing requires an assessment of the interactions of the rates of chemical reactions with the rates of mixing induced by stirring. Mixing by stirring results from the action of convective flow plus any associated turbulence.

The description of the mixing process is further complicated by the necessity of distinguishing mixing and concentration gradients as manifested at the vessel scale—so called macromixing—from those effects manifested at a level approaching the molecular scale—so called micromixing.

The need to quantify deviations from perfect mixing applies both to continuous-flow reactors (conventionally termed CSTRs and PFRs) and to batch or semibatch operation. The theory of mixing appears to be developed to a higher level for flow reactors through the extensive literature on stimulus response. This is deceptive, however, since most mixing models developed from stimulus response are unable to deal adequately with the same situation of separate feed streams of reagents that result in partial segregation within the reactor, whereby parts of the reactor volume are preferentially rich in each of the separate reagents. The same difficulty applies to semibatch reactors where one or more reagents are added continuously to reagents already in the vessel, except that in this case there is no theory equivalent to stimulus response. Indeed, the semibatch case is made the more difficult because the concentration fields of reagents and reactive intermediates vary in both space and time.

The problem of partial segregation was originally handled by simple assemblies of zones of either perfect micromixing or extreme segregation, with the earlier two-zone (Ng and Rippin, 1964) and three-zone (Ritchie and Togby, 1979) models being superceded by a 4-zone structure (Mehta and Tarbell, 1983) comprising pairs of "entering" and "leaving" environments. Other more recent developments have built upon a subdivision of the vessel volume into a perfectly mixed zone associated with an element of plug flow between which circulatory flow takes place (Baldyga and Bourne, 1989) or a closely related configuration that involves interaction and exchange with a mean (backmixed) fluid [the so-called IEM model (David and Villermaux, 1987)]. Both these works (Baldyga and Bourne, 1989; David and Villermaux, 1987) refer specifically to the semibatch operation of a stirred vessel. However, in all these examples, where the reaction and mixing are represented by such a restrictive compartmental division of the reactor, it is difficult to reconcile the structure of the model with the convection and turbulence induced by the stirring action of a typical rotating impeller. The importance of this can already be judged by the observation that the disposition of reagent plumes under semibatch addition is scale sensitive (Bourne and Dell'ava, 1987), so that the reaction zone may be away from or close to the impeller itself. In addition, the overlapping of reagent plumes with multiple addition points results in a loss of selectivity at the expense of productivity, as shown in Bourne and Hilber (1990).

It is also very clear that as the complexity of the reaction kinetics increases, it is necessary to accommodate the mixing in more detail if an accurate prediction of the overall chemical yield performance is to be achieved (Fox and Villermaux, 1990). In this respect, the network-of-zones model, while it sacrifices the greatest detail that could be afforded by solutions of the Navier-Stokes equations (Harvey and Greaves, 1982), provides a very convenient framework for incorporating the effect of multiple reactions. This is because although a reactor may contain thousands of zones, each one being backmixed is described by simple kinetic expressions built up of the locally "perfectly mixed" concentrations. The network-of-zones is moreover computationally convenient, requiring only the solution of first-order ordinary differential equations. One disadvantage of the networks-of-zones used here is that it invokes a simplified uniform representation for the turbulent mixing. This in turn simplifies the algorithm for networks of arbitrary size. In future, this simplification could be improved by importing turbulent exchange flows from CFD solutions of the flow fields, thereby avoiding the current empiricism. This would retain the main advantage of the networks-of-zones model, which is its ability to deal exclusively with concentration fields.

The concept of networks-of-zones was first introduced some time ago and initially developed for a continuous-flow reactor (Patterson and Brodkey, 1975). Applications of the network-of-zones model has progressed from flow follower simulations (Mann et al., 1981), through a description of tracer dispersal and mixing (Mann and Knysh, 1984; Mann et al., 1987), to the most recent work on pairs of reactions (Mann and Wang, 1992; Mann and El-Hamouz, 1991) that exhibit significant partial segregation. As Figure 1 shows, for the reaction scheme $A + B \rightarrow R$ and $A \rightarrow S$ based on a real diazotization coupling reaction (Drain, 1987), as the reagent B is added semibatchwise, there is a "clear B rich zone" predicted to build up from the point of addition. In this case the partial segregation favors the formation of S and reduces the potential yield of R (Mann and Wang, 1992; Nienow et al., 1992).

The network-of-zones model has also been shown to be useful in predicting gas dispersion for a stirred gas-liquid reactor (Mann and Hackett, 1988) and for describing axial and radial solids concentration gradients in single (Brucato and

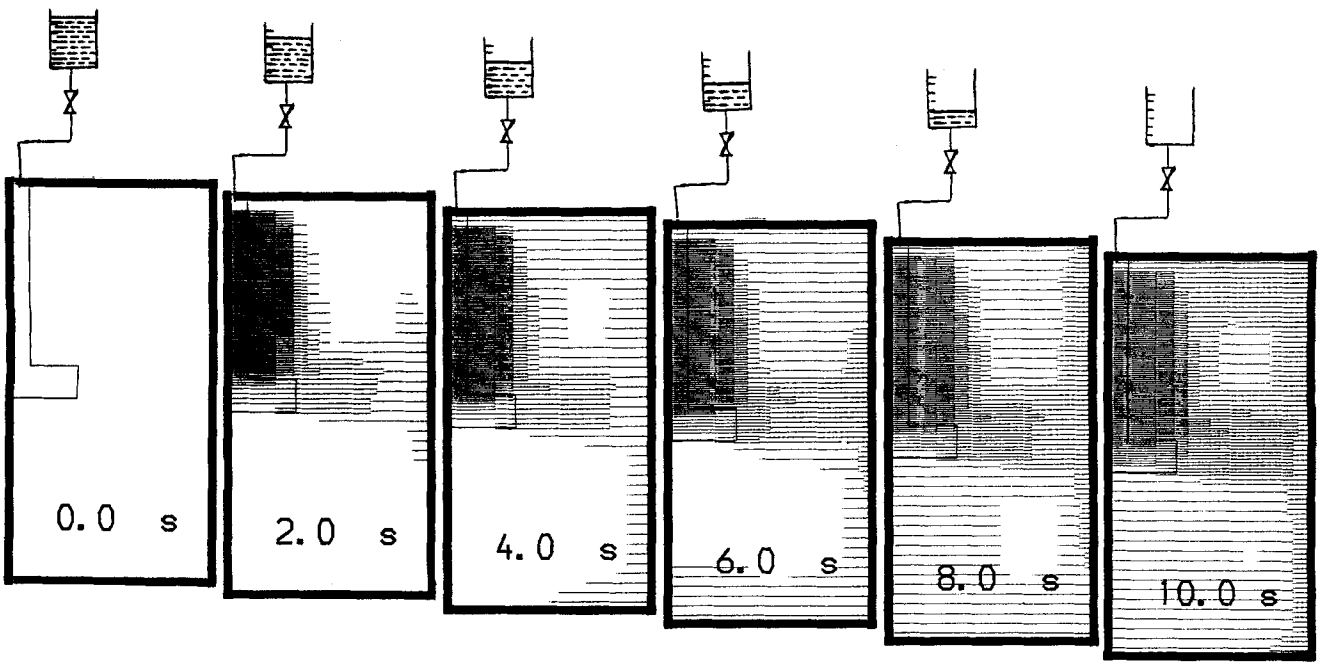

Figure 1. Partial segregation during semibatch addition (Mann and Wang, 1992).

Rizzuti, 1988) and multiple (Brucato et al., 1991) impeller vessels.

This article examines the effects of imperfect macroscale mixing for a triplet set of reactions, using a network-of-zones formulation for a typical stirred reactor fitted with a radial-flow Rushton impeller. The analysis is appropriate for the class of real miscible fluid reactors whose performance is determined only by imperfections in macromixing reflected as concentration gradients on the vessel scale. In these cases the reaction speeds are sufficiently slow to be unaffected by localized micromixing phenomena.

Three Reactions under Perfect Mixing

Before considering the impact of departures from the ideal of perfect mixing, it is appropriate to briefly present the formulation of the perfect mixing equations for a triplet sequence of competitive/consecutive reactions. In line with typical halogenation sequences for hydrocarbons, the reaction scheme under consideration is generally written

$$A + B \rightarrow A\text{-mono-}B \quad \text{or} \quad A + B \xrightarrow{k_1} R$$

$$A\text{-mono-}B + B \rightarrow A\text{-di-}B \qquad R + B \xrightarrow{k_2} S$$

$$A\text{-di-}B + B \rightarrow A\text{-tri-}B \qquad S + B \xrightarrow{k_3} T.$$

Under perfect mixing with mass-action-type kinetics, the kinetic rate equations are

$$\frac{dC_A}{dt} = -k_1 C_A C_B \tag{1}$$

$$\frac{dC_R}{dt} = k_1 C_A C_B - k_2 C_R C_B \tag{2}$$

$$\frac{dC_S}{dt} = k_2 C_R C_B - k_3 C_S C_B \tag{3}$$

$$\frac{dC_T}{dt} = k_3 C_S C_B \tag{4}$$

$$\frac{dC_B}{dt} = -\left(\frac{dC_R}{dt} + 2\frac{dC_S}{dt} + 3\frac{dC_T}{dt}\right). \tag{5}$$

Integration of these equations yields the concentration trajectories of the five components $C_A(t)$, $C_B(t)$, $C_R(t)$, $C_S(t)$, and $C_T(t)$. Of particular interest for practical batch processing is the instantaneous fractional yield of a product I with respect to reagent A denoted by $\varphi(I/A)$, following the nomenclature of Denbigh (1966).

This is defined by

$$\varphi\left(\frac{I}{A}\right) = \frac{\text{rate of production of } I}{\text{rate of consumption of } A} = \frac{dC_I/dt}{-dC_A/dt} = \frac{dC_I}{-dC_A}. \tag{6}$$

For the initial product R this is given by

Table 1. Simulation Parameters at Laboratory Scale

Initial conc. of A	C_A^0	0.02 kmol·m^{-3}
Feed conc. of B	C_B^f	1.80 kmol·m^{-3}
Semibatch addition rate	q_B^f	12.5×10^{-6} m^3·s^{-1}
Semibatch addition time	t_a	80 s
Vol. of B added	V_B	0.01 dm^3
Vessel vol.	V	0.3 dm^3
Std. Rushton turbine	D	24.1 mm
Reaction rate constants	$k_{1,2,3}$	500 m^3·kmol^{-1}·s^{-1}
Network size	N	$(20\times20)+(20\times40)$
Feed position	i^*,j^*	1, 58

$$\varphi\left(\frac{R}{A}\right) = \frac{k_1 C_A C_B - k_2 C_R C_B}{k_1 C_A C_B} = 1 - \frac{k_2 C_R}{k_1 C_A} \tag{7}$$

so that the relative yield of product R is independent of the concentration of B. This means that the relative yield of R and the other products S and T are quite independent of the rate of addition of reagent B under semibatch operation where B is added to A. In effect the rate of addition of B determines the absolute timewise sequence of the individual products, but does not in any way affect the relative positions of each of the reagent and product trajectories.

By way of illustration, we shall examine the behavior of an isothermal laboratory reactor of volume 0.3 dm^3 stirred by a Rushton turbine using the data values presented in Table 1. The results for a semibatch addition of B over 80 seconds are then shown in Figure 2 where the charge of B is three times the initial molar charge of A, so that the reaction proceeds through to complete reaction to the final product T. With $k_1 = k_2 = k_3 = 500$ m^3·kmol^{-1}·s^{-1}, the concentration trajectory of A shows an approximately first-order disappearance. The first product R reaches a maximum at 0.36 C_A^0 after about 25 s and the second product S peaks at 0.28 C_A^0 after some 50 s. The final product T accumulates progressively at an accelerating rate up to an inflexion point of around 78 s. In line with the use of equal rate constants, the final product T only begins to appear at an appreciable level after the primary and secondary products have passed sequentially through their maximum values. These maxima of

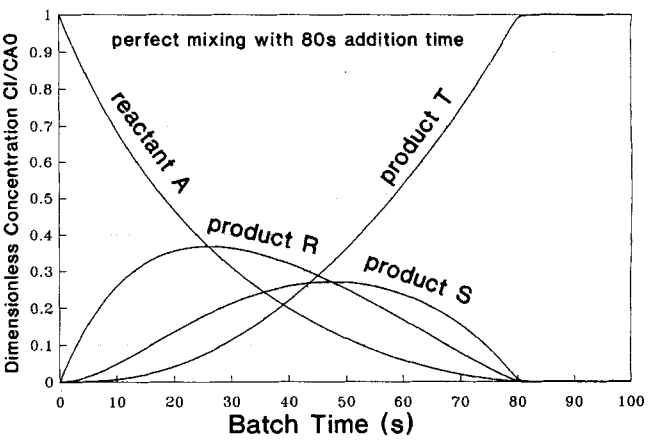

Figure 2. Reaction trajectories for perfect mixing.

the intermediates R and S are clearly separated, with the second product maximum following the first one.

The result of the independence of $\varphi(R/A)$ upon C_B as shown in Eq. 7 suggests that there could be no interest in the variation of the rate of addition of reagent B. This is only true, however, provided that the predicted assumption of perfect mixing is reasonably valid.

In practice, under semibatch addition of B to A, the local concentration of B near the addition point will be the result of the three-way interaction of the addition flow rate, the local flow generated by the impeller (which serves to dilute the incoming addition stream), and the local disappearance rate of B due to participation in the reactions.

This nonuniformity of B is clearly evident in Figure 1 where a "cloud" of fluid rich in B builds up toward the impeller as addition proceeds near the surface, a result previously calculated for a simpler pair of reactions (Mann and Wang, 1992). Wherever the local concentration of B is high, the primary reagent A and the initial product R can become locally depleted by reaction. This depletion can obviously in principle be sufficient to affect $\varphi(R/A)$ in Eq. 7, since the effect on each of A and R is not likely to leave the ratio C_R/C_A equal to that applicable to the perfect mixing case. The same argument can be extended to the other product yields $\varphi(S/A)$ and $\varphi(T/A)$. Under imperfect mixing conditions, it can then be expected that local regions rich in B will give rise to distortions of the product distribution.

In order to predict the effects of the interactions of internal mixing and addition rate of B upon this triplet sequence of reactions, it is necessary to set up a valid model of the interactions themselves that can account for the finite rates of mixing, flow, and reaction that are present in real cases.

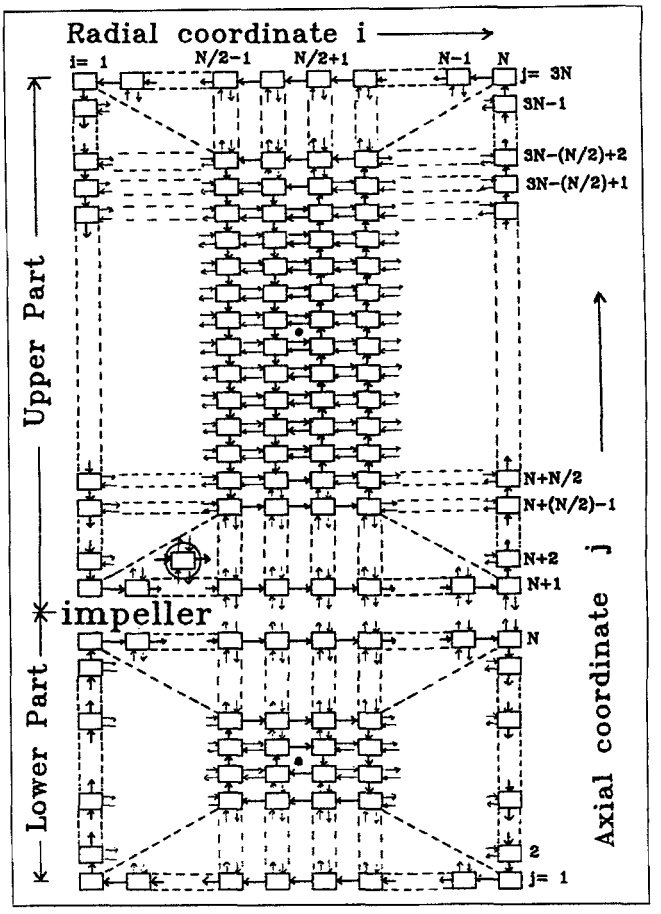

Figure 3. Network of zones.

Formulation of a Network-of-Zones Analysis

Figure 3 shows a modified form of the previous network-of-zones (Mann and Knysh, 1984; Mann et al., 1987) that accommodates the impeller at a clearance above the base of $c = H/3$. For this one-third clearance positioning, there is an $N \times N$ set of zones below the impeller and a set of $N \times 2N$ zones above the impeller. There are then $N/2$ concentrically nested flow loops below the impeller as well as above it. Figure 3 shows the two innermost flow loops around each of the upper and low focii of circulation. In Figure 3 the outermost flow loops above and below the impeller are shown partially complete, which is indicative of the general case for arbitrary N values. The impeller is located between $j = N$ and $j = N + 1$. The focus of the lower circulation loop is located between $i = N/2$ and $N/2+1$ and $j = N/2$ and $N/2+1$. The upper flow loop focus is then found between $i = N/2$ and $N/2+1$ and $j = 2N$ and $2N+1$.

It is possible to introduce any form of internal velocity profile by allocating the overall impeller-generated flow equally among the flow loops (totaling N) and adjusting the set of zone volumes accordingly. However, earlier work (Mann and Knysh, 1984) showed that such volume manipulation to adjust the velocity profiles made almost no difference to the mixing behavior when compared with the simple equal-volume case. This is equivalent to the mixing being dominated by the overall convection rate of the impeller.

With $N = 20$, the set of zones of equal volume appear as shown in Figure 4. This $(20\times20)+(20\times40)$ assembly comprises 1,200 zones in total. Each backmixed zone experiences an equal and opposite exchange flow with adjacent zones in adjacent loops (except, obviously, for the innermost and outermost loops, with the further exception when the two outermost loops lie adjacent to one another at the junction between the upper and lower circulations). The equal and opposite exchange flows are always "orthogonal" to the mean circulatory flow and conceptually are meant to simulate the effect of turbulence acting to create mixing between parallel flowing convection steams.

Semibatch Addition of Reagent B

In line with earlier discussions, the vessel is envisaged as holding an initial charge of reagent A, with B to be added in concentrated form semibatchwise over an addition time period t_a.

For an arbitrary i, j zone, such as the zone $(3, N+2)$ shown ringed in Figure 3, in which the convective flow in a loop is outward (in the direction of increasing i), an unsteady material balance for a component I is based on

Accumulation = input by flow and exchange

$-$ output by flow and exchange $\pm$ rate of reaction

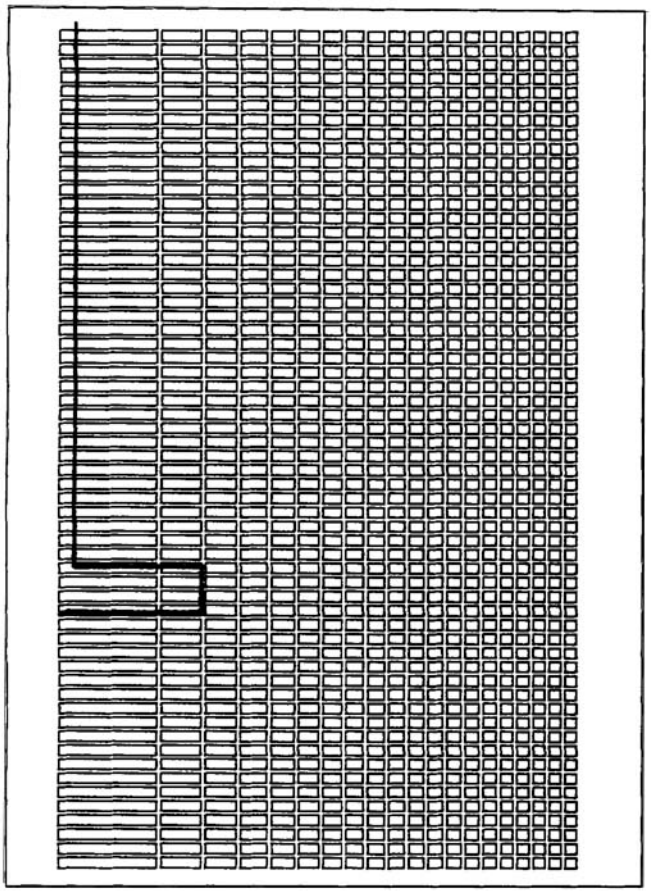

Figure 4. Set of 1,200 equal volume zones forming a (20×20)+(20×40) configuration.

in which case

$$\frac{dC_{Ii,j}}{dt} = \frac{q}{V_{i,j}}[C_{Ii-1,j} - (1+2\beta)C_{Ii,j} + \beta(C_{Ii,j+1})] \pm r_{Ii,j}. \tag{8}$$

For the triplet reaction sequence, the rate expressions for each component relate to those already set out for the perfect mixing case in Eqs. 1 to 5, so that

$$\begin{aligned} r_{Ai,j} &= -k_1 C_{Ai,j} C_{Bi,j} \\ r_{Ri,j} &= k_1 C_{Ai,j} C_{Bi,j} - k_2 C_{Ri,j} C_{Bi,j} \\ r_{Si,j} &= k_2 C_{Ri,j} C_{Bi,j} - k_3 C_{Si,j} C_{Bi,j} \\ r_{Ti,j} &= k_3 C_{Si,j} C_{Bi,j} \\ r_{Bi,j} &= -(r_{Ri,j} + 2r_{Si,j} + 3r_{Ti,j}). \end{aligned} \tag{9}$$

Equation 8 applies to every component in every zone, except for zone i^*, j^*, which is assumed to be the addition point for the semibatch addition of B. For a linear addition rate of B given by q_B^f the input term for B in the i^*, j^* zone is given by the product $C_B^f\ q_B^f$ over the addition period t_a.

The initial conditions at commencement of addition are

$$\begin{aligned} C_{Ai,j} &= C_A^0 \quad \text{for} \quad 1 \le i \le N \\ C_{Bi,j}, C_{Ri,j}, C_{Si,j}, C_{Ti,j} &= 0 \quad \text{and} \quad 1 \le j \le 3N. \end{aligned} \tag{10}$$

The set of Eqs. 8 for all i, j and $I = A$, B, R, S, and T are integrated from the initial conditions of Eq. 10 using any convenient integration routine. For the case of $N = 20$, this triplet sequence of reactions requires the solution of 6,000 first-order ordinary differential equations (odes).

Imperfect Mixing at the Laboratory Scale

A simulation will now be examined using an addition time for B of 80 s. This provides a direct comparison with the perfect mixing case previously outlined.

The overall flow rate generated by the impeller at a stirrer speed of 463 rpm will be obtained from

$$Q = 2.75\, nD^3 \tag{11}$$

as suggested by Oldshue (1983), and in the present calculations it will be assumed that this overall flow is allocated two-thirds to the upper circulation and one-third to the lower circulation. As a result, the average circulation times are identical above and below the impeller. A network configuration of (20×20)+(20×40) will be adopted with a turbulent exchange parameter value of $\beta = 0.2$, except for the impeller zones where a value of $\beta = 10$ is used, in line with previous simulations of tracer mixing behavior (Mann and Knysh, 1984; Mann et al., 1987). Using a feed concentration of B of $C_B^f = 1.8$ kmol·m^{-3} requires a linear addition rate of B of $q_B^f = 5 \times 10^{-6}$ m^3 s^{-1}.

In constructing sectional concentration fields, the following horizontal shading convention for each zone will be applied (Mann and Wang, 1990; Mann and El-Hamouz, 1991) to any component I:

No. of Lines	Concentration Range
5	$C_I/C_A^0 \ge 0.9$
4	$0.7 \le C_I/C_A^0 < 0.9$
3	$0.5 \le C_I/C_A^0 < 0.7$
2	$0.3 \le C_I/C_A^0 < 0.5$
1	$0.1 \le C_I/C_A^0 < 0.3$
0	$0 \le C_I/C_A^0 < 0.1$

Figure 5a then shows the computed concentration fields for B over five time intervals from the initial condition to the completion of the addition of B semibatchwise. The plume of reagent B appears as a sectional image reconstruction using the shading convention outlined earlier.

After 16 s, when one-fifth of the B has been added, B is only detectable at a concentration greater than 0.1 C_A^0 in three zones with a maximum of three lines in the addition zone (i^*, $j^* = 1$, 58) just below the liquid surface where $C_B/C_A^0 \le 0.7$ but > 0.5.

By the time four-fifths of the B has been added at 64 s, the cloud of B, or reagent plume as it appears by shading, has enlarged over about 15 zones. On completion of the addition

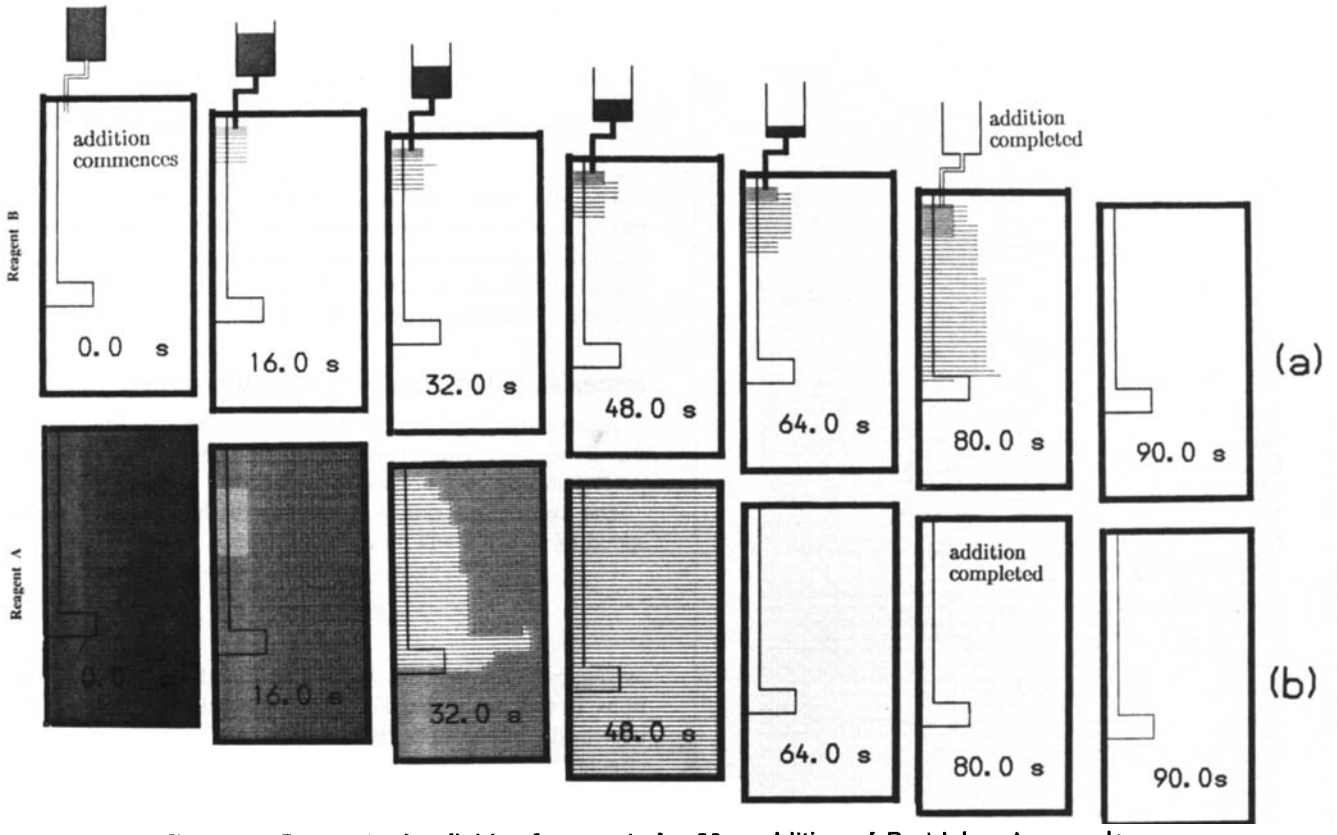

Figure 5. Concentration fields of reagents for 80 s addition of B at laboratory scale.

(a) Distribution of the "added" reagent B. (b) Distribution of the "charged" reagent A.

at 80 s, there is a large distinguishable plume of B that extends as far as the impeller. The highest concentration at this point extends over two zones with $0.7 \leq C_B/C_A^0 < 0.9$, at one zone below the addition point. Mixing and reaction continue on cessation of addition, but after a further 10 s (equal to ten interval turnovers of the batch fluid), that is, at 90 s, $C_B < 0.1\ C_A^0$ throughout the vessel so that no shading is present on the final sectional image.

There is a corresponding evolution of a counterpart concentration field for the primary reagent A throughout the semibatch addition. The set of image reconstructions for A, using the same shading convention, are set out in the same ways as for B in Figure 5b.

Reagent A initially fills the whole vessel at its initial concentration C_A^0, with every zone shaded with five horizontal lines. After 16 s, when one-fifth of the B has been fed, there is already a significant depletion of reagent A. The nonuniformity of A is relatively more pronounced at 16 s. Over the first 32 s or so, the nonuniformity of reagent A is more pronounced than for reagent B. This is because A is continually swept through the zones close to the addition point by convective flow. Reagent A is reacted and then convected on toward the impeller. The concentration field of A shows a developing depletion, while B forms a smaller pseudostationary flame or plume, which is initially just confined to a few zones below the injection point.

This pattern reverses itself, however, during the second half of the addition. The plume of reagent B continues to grow while the zones relatively depleted in A shrink. On completion of the addition, A is undetectable at $C_A < 0.1\ C_A^0$, but the plume of B has enlarged down to the impeller and is shaded at $C_B \geq 0.1\ C_A^0$ in some 150 zones.

The degree of the nonuniformity of A affects the instantaneous fractional yield of R denoted by $\varphi(R/A)$ in every cell, as indicated by Eq. 7. This then shows up as a loss in the overall fractional yield of R given by

$$\varphi\left(\frac{R}{A}\right) = \frac{\text{mol of } R \text{ produced}}{\text{mol of } A \text{ consumed}} - \frac{\overline{C}_R}{C_A^0 - \overline{C}_A} \tag{12}$$

where the instantaneous overall average concentration of a component I is given by

$$\overline{C}_I = \frac{1}{3N^2} \sum_{i=1,j=1}^{i=20,j=60} C_{Ii,j}, \tag{13}$$

which is equivalent to the instantaneous mixed concentration as averaged over the vessel. The associated losses in overall yield can be discerned from Figure 6, which effectively shows $\overline{C}_I$ for each component vs. time and allows a comparison between the network-of-zones model for imperfect mixing and the results for assumed perfect backmixing. Focusing on the

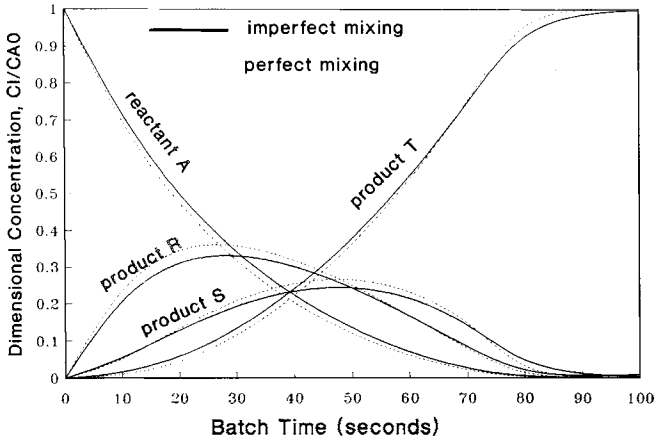

Figure 6. Comparison of perfect mixing with network-of-zones predictions for 80 s addition of *B*.

Trajectories in time at laboratory scale.

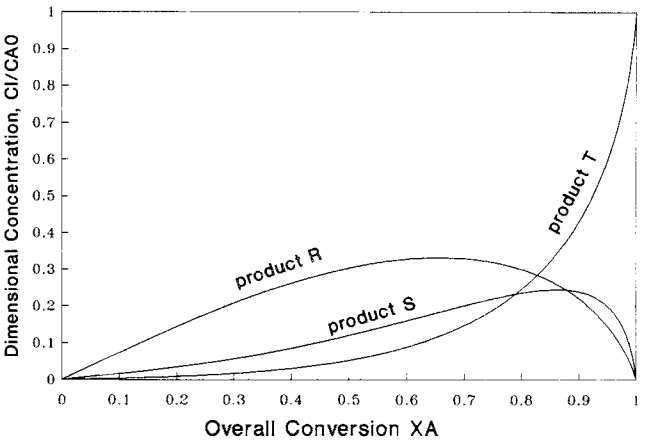

Figure 8. Network-of-zones prediction for 80 s addition of *B*.

Product trajectories vs. conversion at laboratory scale.

first product R, Figure 6 shows that after about 25 s the overall average concentration of R has been reduced to 0.33 C_A^0 from its perfect mixing value of 0.36 C_A^0. This amounts to a 10% loss of the prospective amount of R compared to the perfect mixing case. This loss of R is a result of the less than perfect mixing depicted in the sequences of sectional images shown in Figure 5a and b.

Figure 7 then shows the consequent spatial distribution of the instantaneous fractional yield of R over the whole vessel after 16 s. The values of $\varphi(R/A)$ show small but significant departures from uniformity across the vessel, confirming that the laboratory scale vessel is reasonably close to perfectly backmixed. The spatial variation in $\varphi(R/A)$ is obviously more marked than the overall small reductions in $\overline{C_R}$ indicated in Figure 6. Thus $\varphi(R/A)$ varies from a minimum of 0.34 to a maximum of 0.58.

However, it is clear from Figure 6 that under this degree of imperfect mixing, the sequence whereby the primary product appears initially, followed by the second product and thereafter the third product is exactly in line with the qualitative behavior for the initial sequential appearance of mono-, di- and triproducts expected from perfect mixing. An alternative way to present this result is shown in Figure 8, which uses the conversion of A instead of time as the abscissa.

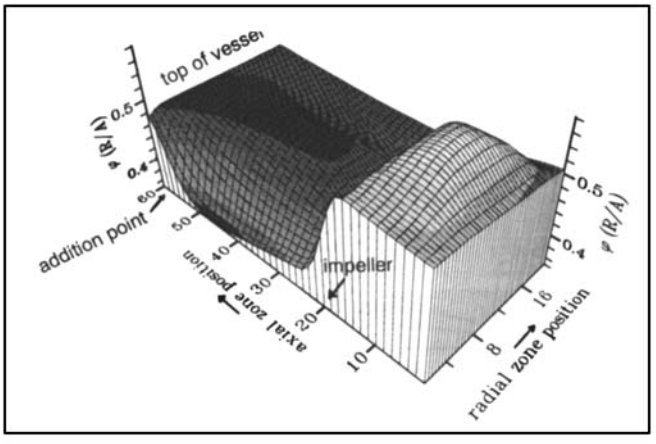

Figure 7. Spatially distributed instantaneous fractional yields for primary product *R*.

Imperfect Mixing at Semitech Scale (30 dm³)

If the scale of the vessel is increased at equal tip speed, we can anticipate that a relatively more intense cloud or plume of B will be seen. Full details of the evolving concentration field of B, while all other conditions are maintained, are shown in Figure 9a. The detectable field of B delineated by the single shading of zones for which $0.1 \leq C_B/C_A^0 < 0.3$ is always much larger than for the smaller laboratory reactor.

For the same addition time of 80 s, the behavior of the concentration fields of B and A, as shown in Figures 9a and b, show an increased departure from perfect mixing compared with Figures 7a and b. On completion of the addition of B after 80 s, the plume of added B passes through the impeller, and the greatest possible concentration of B with $C_B \geq 0.9\ C_A^0$ now evidently extends part way down to the impeller itself. There is no multiple shading of zones beyond the impeller tip, so that the "visible" plume extending beyond the impeller only has $C_B < 0.3\ C_A^0$. The situation with respect to reagent A obviously reflects this more pronounced segregation behavior of B. Thus in Figure 9b, after one-fifth addition of B at 16 s, there is no region without some shading as compared to the absence of shading below the point of addition in the corresponding Figure 7b.

The intermediate behavior of the overall averaged concentrations is then shown in Figure 10. Product R and product S appear with maxima—R is at $\overline{C_R} = 0.18\ C_A^0$ and S is at $\overline{C_S} = 0.13$—which is similar to the laboratory scale case. However, it is now clear that triproduct T accumulates after the initial appearance of R, but in advance of the accumulation of S. Simplistically, with assumed perfect mixing, this case has apparent reaction kinetics of the form

$$A + B \xrightarrow{k_1} R + B \xrightarrow{k_2} S + B \xrightarrow{k_3} T,$$

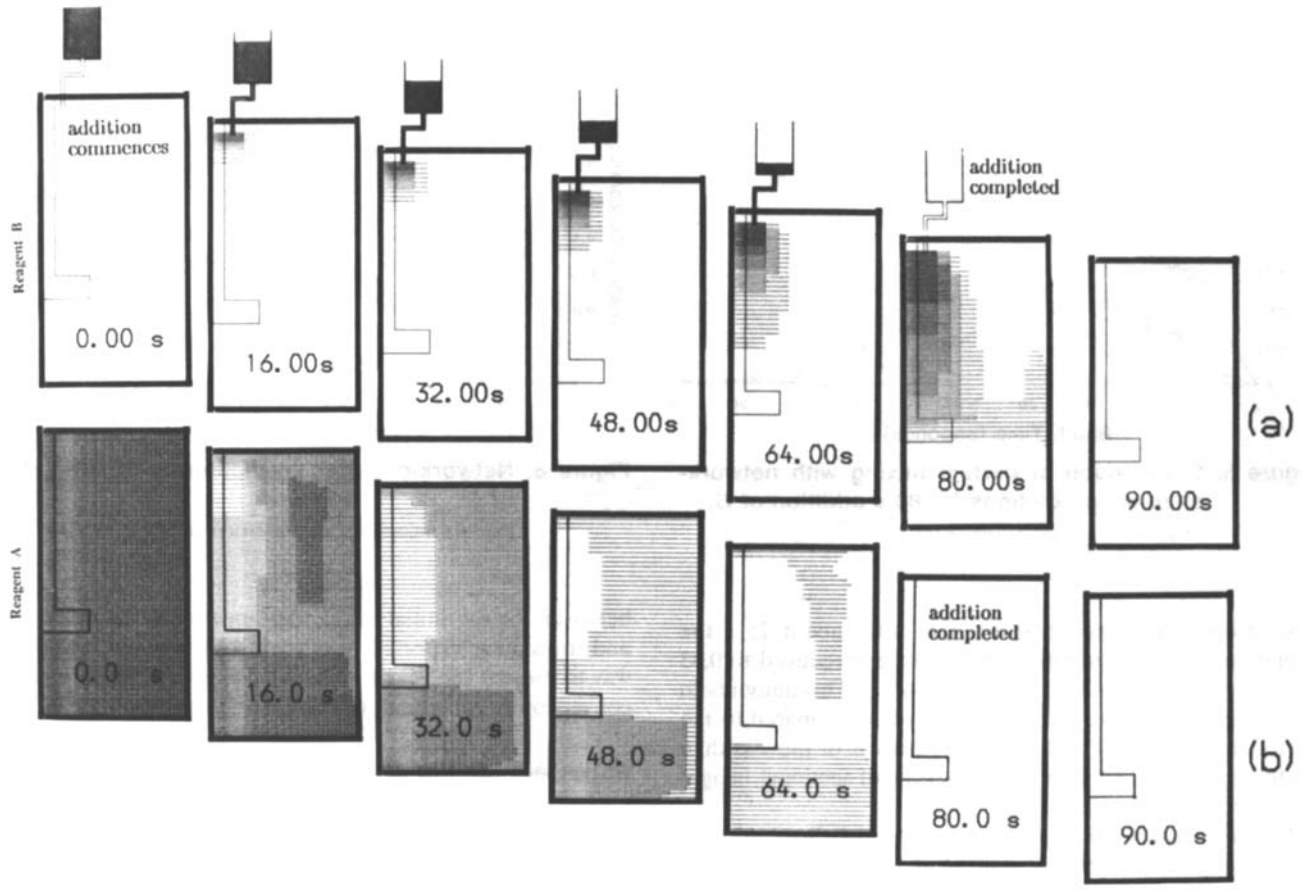

Figure 9. Concentration fields of reagents at semi-tech scale.

(a) Distribution of the "added" reagent B. (b) Distribution of the "charged" reagent A.

with T seemingly formed directly by a "shunt" from R. The qualitative explanation for this is that it arises from localized overreaction as a result of a locally high concentration of B.

Imperfect Mixing at Production Scale (3,000 dm^3)

At the production scale of 3,000 dm^3, the stirrer speed has been reduced to 21.5 rpm to provide for equal tip speed. The evolution of the spatial concentration fields is shown in Figure 11a and b.

When one-fifth of the B has been added at 16 s, it can be seen that $C_B \geq 0.9\ C_A^0$ in about twenty zones. On completion of addition at 80 s, $C_B \geq 0.9\ C_A^0$ in zones extending as far down as the impeller, which now number about 300. This is in complete contrast to the laboratory scale case for which no zones exhibited this strength of B. Altogether at completion of addition, $C_B \geq 0.1\ C_A^0$ in some 500 zones, mostly in the upper part of the vessel. The plume of B extends through the impeller and is detectable close to the wall above and below it. It extends further up the wall above the impeller, because A is more depleted in the upper part of the vessel. This is a consequence of B being added just to the convective flow above the impeller. After a further 10 s, following the shutting off of B, the plume is swept onward around the vessel and continues to be depleted by the continuing reaction, so that at 90 s a concentration of $C_B \geq 0.1\ C_A^0$ is still clearly detectable in a relatively slowly diminishing volume.

The behavior of the concentration field of B is obviously complemented by a correspondingly more severe local depletion of reagent A, as shown in Figure 9b. The very intensive partial segregation of B is obviously reflected in the sequence of sectional concentration fields of A in this figure.

At one-fifth addition after 16 s, severe depletion of A gives

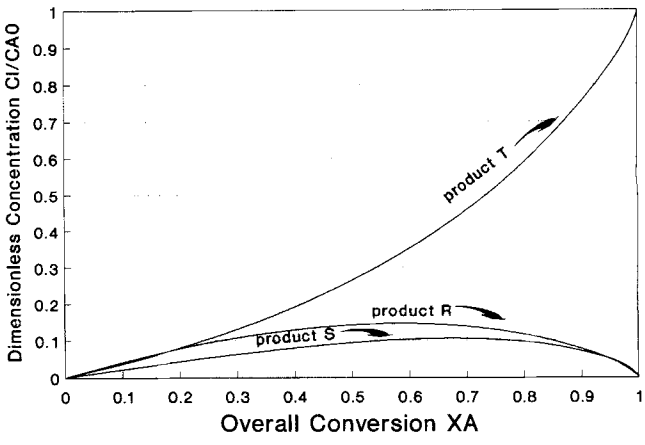

Figure 10. Network-of-zones predictions at semitech scale.

Product trajectories vs. conversion.

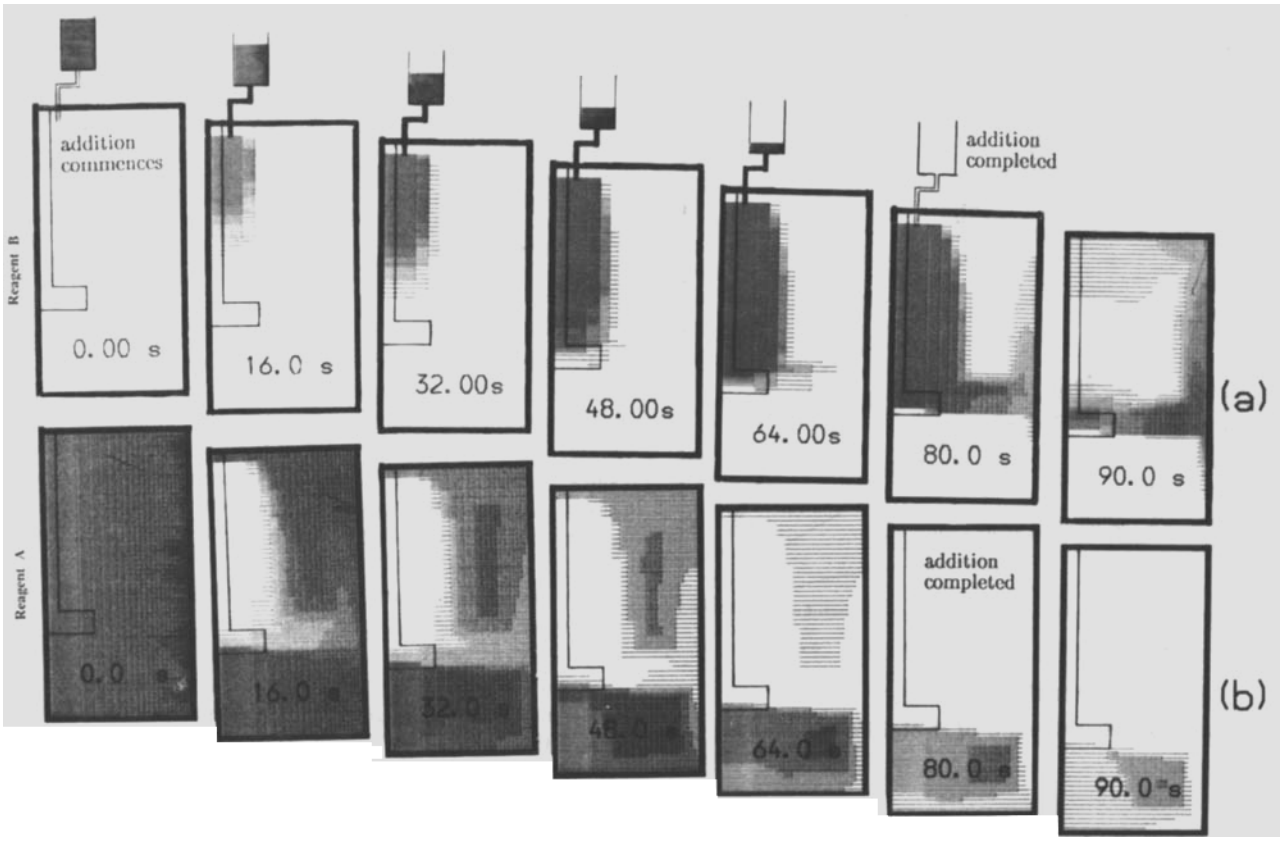

Figure 11. Concentration fields of reagents at production scale.

(a) Distribution of the "added" reagent B. (b) Distribution of the "charged" reagent A.

$C_A < 0.1\ C_A^0$ in the sixty or so unshaded zones just below the addition point, so that these zones form a hole of almost completely reacted A. Circulating convected fluid relatively depleted in A now stretches through and beyond the impeller. The relative depletion of A is again much more evident than the corresponding plume of B.

On completion of addition at 80 s, the upper part of the vessel has $C_A < 0.1\ C_A^0$ and the lower part has $C_B < 0.1\ C_A^0$. Mixing and stirring for a further 10 s beyond the completion of addition shows that ongoing reaction has depleted $C_A < 0.1\ C_A^0$ in only a few further zones, confirming that the relatively slower overall convection at the production scale gives rise to only slowly continuing reaction.

The overall result in terms of the integrated average concentration of each component $\bar{C}_I$ is then shown in Figure 12. It is immediately obvious that the sequence of appearance of each product has now reversed when compared with the result for laboratory scale addition in Figure 8. The triproduct T now accumulates in the batch in advance of both the mono- and diproducts. This is an apparent paradox since it appears as if the triproduct is produced by chemical reaction faster than the initial monoproduct. Products R and S still pass through maxima in sequence in a way that would be logical except for the apparently direct faster reaction to the triplet product.

Such behavior is impossible under perfect mixing unless one presupposes that some hypothetical fast reaction to the final product were to somehow bypass, by a parallel path, the normal progressive sequence of product formation. The kinetic scheme would need to have the appearance

$$\overset{k^1}{\Big\lceil\!\!\Big\rceil}\qquad A + B \overset{k_1}{\rightarrow} R + B \overset{k_2}{\rightarrow} S + B \overset{k_3}{\rightarrow} T$$

such that the triplet addition or substitution were instanta-

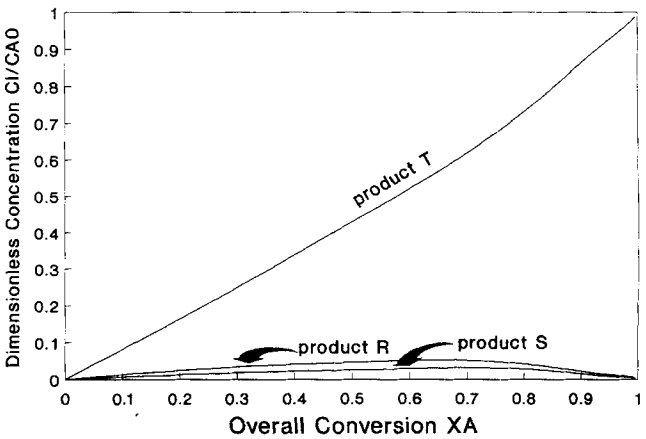

Figure 12. Network-of-zones predictions at production scale.

Product trajectories vs. conversion.

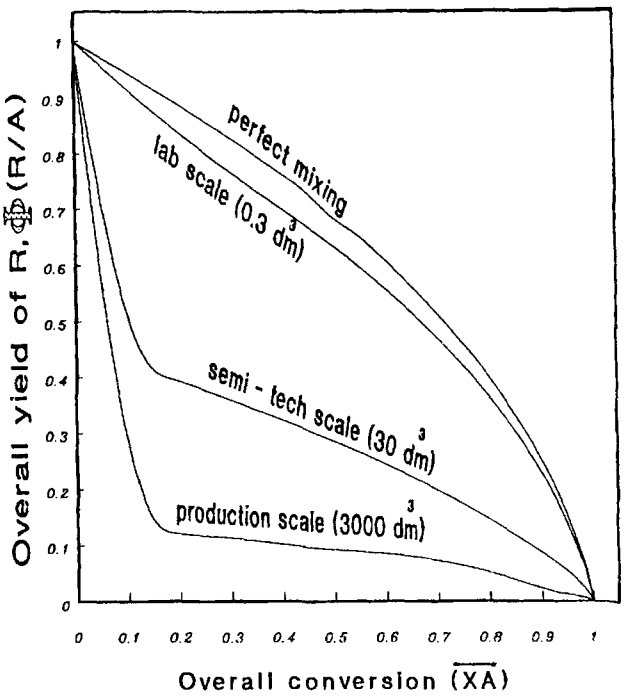

Figure 13. Overall yield of *R* at different scales.

neous. The resolution of the paradox is of course already obvious from the concentration fields in Figures 11a and 11b. The much more intense concentration of B below the point of addition causes the sequence of reactions to advance locally almost to completion to the final product, so that its integrated average rate of appearance (over the whole vessel) is in excess of the overall rates to R and S. It is nevertheless profoundly interesting that a set of semibatch product trajectories that confound classic chemical reaction kinetics can be explained by a simple, albeit massive, departure from perfect mixing.

It can be readily concluded that the effect of imperfect mixing gives rise to a whole range of possible distortions of the product distribution, some of which appear paradoxical with reference to perfect mixing and a sequence of competitive/consecutive reactions. The three examples presented over a typical scale-up range have been chosen to exemplify

- A conventional appearance of the final product following the first and second products;
- The appearance of the final product ahead of the secondary one, but lagging the primary one;
- The extreme case where the final product appears in advance of both the primary and secondary products.

Overall Yields of *R*, *S*, and *T*

Finally, it is worth noting the characteristic behavior of the overall yield of a product I with respect to the charged reactant A denoted by $\Phi(I/A)$, in the face of variations of the scale of operation.

Figure 13 shows $\Phi(R/A)$ vs. the conversion of A, the conditions and parameters being as set out in Tables 1 and 2.

Table 2. Scaling Up at Equal Tip Speed

	Lab.	Semitech	Prod.
Vessel vol., dm³	**0.3**	**30.0**	**3,000.0**
Vessel dia., mm	72.5	336.6	1,563.2
Turbine dia., mm	24.1	112.2	521.0
Turnover time, s	1.0	4.6	21.3
Stirrer speed, rpm	463.0	100.0	21.5
Internal flow, $m^3 \cdot s^{-1}$ ($\times 10^3$)	0.3	6.5	140.0
Tip speed (ND), $m \cdot s^{-1}$	**0.186**	**0.186**	**0.186**

For the primary product R, the overall yield is always highest with perfect mixing, falling in a convex fashion to zero yield at complete conversion. Even at the smallest laboratory scale, real mixing rates as simulated by the network-of-zones shows a more concave behavior, especially at lower conversions. At production scale, the overall yield of R falls very rapidly to a low value of 0.1 even at the low conversion of A of 0.2.

For the intermediate product S, which contains 2 mols of B, a quite complex pattern of overall yield is observed in Figure 14. Perfect mixing is evidently highly disadvantageous, the corollary being that departures from perfect mixing are beneficial and a degree of partial segregation of B can vastly improve the yield of S at lower conversions. Perfect mixing becomes more favorable at much higher conversion levels. Figure 14 suggests the interesting possibility of maximizing the yield of S at high conversion by using a controlled degree of partial segregation of B by adjusting the intensity of mixing as the semibatch addition progresses.

Finally, Figure 15 is a counterpart to Figure 13, since here the worst yield of the final product T, denoted by $\Phi(T/A)$, is obtained with perfect mixing. Improved yields are secured at the larger scale, which results in an always favorable partial segregation. This partial segregation causes the yield curve to become more convex relative to the concave behavior of per-

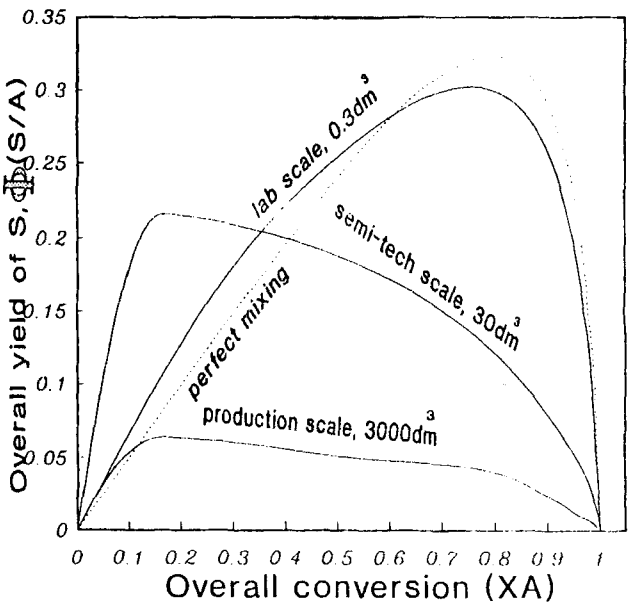

Figure 14. Overall yield of *S* at different scales.

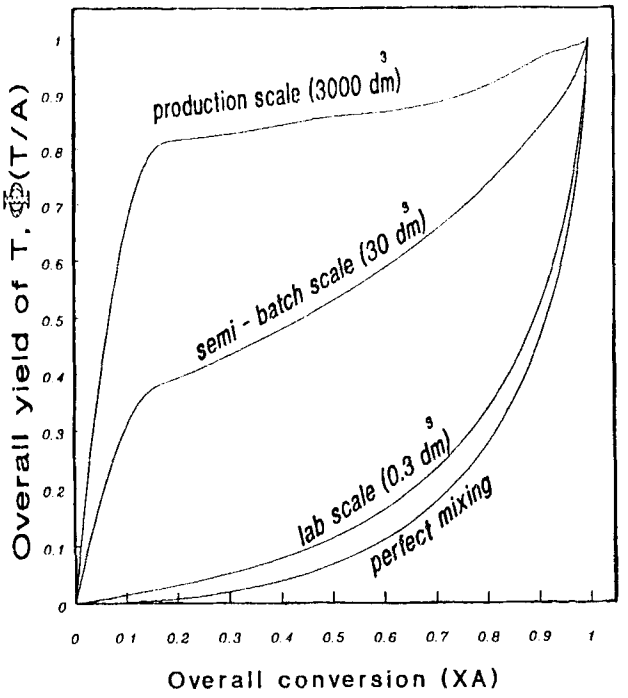

Figure 15. Overall yield of *T* at different scales.

fect mixing, so that high yields of T can be achieved at relatively low extents of conversion. Distinctively, for the final product, large-scale operation favors both yield and productivity simultaneously.

Validity of the Locally Perfect Micromixing Assumption

The relative importance of micromixing can be examined with respect to the value of a micromixing modulus M. The value of this modulus reflects the comparative rates of diffusion and reaction on the contacting of miscible fluid streams at different concentrations. The definition of the modulus (see, for example, Bourne and Rohani, 1983) starts from the level of energy dissipation as given by

$$\epsilon = P_0 n^3 D^5 V^{-1}, \tag{14}$$

which in turn defines a turbulent microscale dimension

$$\lambda_k = (\nu^3 \epsilon^{-1})^{0.25}. \tag{15}$$

The corresponding reaction thickness is then

$$\delta_0 = \beta(\lambda_k/2) \tag{16}$$

and the micromixing modulus M is obtained by

$$M = k_2 C_B^f \delta_0^2 \mathfrak{D}_B^{-1}. \tag{17}$$

The appropriate value of β in Eq. 16 has been shown to be somewhat dependent on the feed pipe position (Bourne et al., 1981) taking values $0.1 < \beta < 0.14$ below the impeller, $0.2 < \beta < 0.26$ at the impeller, and $0.3 < \beta < 0.39$ for the liquid surface.

Taking a representative value of $\beta/2 = 0.15$ for the additions simulated here, Table 3 shows the calculated values of M. The highest value of $M = 46$ occurs for the production scale. In order for micromixing to begin to affect the intrinsic chemical selectivity, the value of the modulus should exceed a value of 50 (Belevi et al., 1981). The values of M in Table 3 show that micromixing effects should be negligible. This is mainly a result of the relatively low value of the reaction rate constant k_2 taking a value of only 500 kmol $m^{-3}s^{-1}$ for the primary $A + B$ reaction. A value of the diffusivity of $\mathfrak{D}_B$ of 9×10^{-9} $m^2 \cdot s^{-1}$ corresponds to a typical value for bromine in a low viscosity hydrocarbon fluid, so that the $A + B$ reaction corresponds to the miscible bromination of a hydrocarbon. Practical examples of product distribution distortions for such reactions prompted the work described in this article (Haywood, 1990).

In any case, Table 3 may possibly somewhat exaggerate the potential impact of the micromixing effect, because it is based upon the undiluted feed composition of B, C_B^f. Within the vessel, the localized concentrations of B are mostly about three orders of magnitude ($\times 1{,}000$) smaller than this (external) feed value, so that over most of the vessel the M values would be reduced by this factor. On the other hand, the potential to exaggeration in Table 3 will be to some extent countered by uncertainty over local values of turbulence intensity close by the feed tube. Certainly for the feed tube position used here (i^*, $j^* = 1$, 58) close to the impeller shaft in the upper vessel, the local rate of energy dissipation should be much less than the average over the whole vessel. Care should therefore be exercised in discounting micromixing effects based upon average turbulent dissipation rates.

The values of the micromixing modulus in Table 3 therefore seem to confirm that the triplet sequence of competitive/consecutive reactions used here represent a (not unrealistic) case of complex reactions being affected by macroscale concentration gradients produced as a result of the interactions of (relatively) slow reaction rates with the rates of internal convection and mixing induced by the Rushton turbine impeller. The illustrations of product selectivity distortion thereby arise solely from macromixing, with the rates of local diffusion being sufficiently fast as to provide negligible localized concentration gradients. This result is in contrast to the widely adopted diazotization coupling reaction. This is more severely micromixing influenced because the second reaction rate constant takes a higher value of 7,000 $kmol \cdot m^{-3} \cdot s^{-1}$, which is some fourteen times greater than the rate constant values used in this study.

Table 3. Micromixing Modulus at Three Scales

	Lab.	Semitech	Prod.
Vessel vol., dm^3	0.3	30	3,000
Vessel dia., mm	24.1	112.2	521.0
Stirrer speed, rpm	463	100	21.5
Feed concn of B, $kmol \cdot m^{-3}$	1.8	1.8	1.8
Energy dissip. rate, $J \cdot kg^{-1} \cdot s^{-1}$	0.062	0.014	0.003
Reaction thickness, μm	10.0	14.6	21.5
Micromixing modulus	10.1	21.5	46.2

Conclusions

1. A modified version of the network-of-zones model, which uses a $(N \times N)+(N \times 2N)$ configuration to accommodate the positioning of a radial flow impeller at a clearance of $c = H/3$, can be applied to evaluate the effect of imperfect mixing on the triplet sequence of reactions:

$$A + B \overset{k_1}{\rightarrow} R + B \overset{k_2}{\rightarrow} S + B \overset{k_3}{\rightarrow} T.$$

2. Under semibatch addition of B to a vessel charged with reagent A, networks-of-zones permit an evaluation of the interaction of internal convection with addition flow rate and its consequences for each of the products R, S, and T as reaction in the batch proceeds.

3. For a $(20 \times 20)+(20 \times 40)$ division of the reactor volume, a representative set of parameters shows how the degree of partial segregation of reagents A and B is affected by scaling-up at equal tip speed and how the extent of this partial segregation affects the localized instantaneous yield and the overall yields of the three possible products. The set of $(20 \times 20)+(20 \times 40)$ zones requires the integration of 6,000 first-order differential equations.

4. The partial segregation of A and B can be conveniently visualized using a simple degree of shading for each zone in the network, providing for a sectional image reconstruction of the concentration field.

5. The concentration trajectories of each of the products can show an apparently paradoxical behavior. Under perfect mixing, the primary product must appear initially ahead of the second product, which is then followed by the final product. For very strong segregation of A and B, at production scale, it is shown that it is possible for the final product to appear initially well ahead of the first and second products, even though in passing through maxima, the primary and secondary products show a behavior in accordance with simple chemical kinetics. At a very small scale, typical of laboratory testing, the behavior of product trajectories is qualitatively close to that expected for perfect mixing. At an intermediate semitech scale, an attenuated paradox can be observed, whereby the final product appears after the first one, but ahead of the second one.

6. The overall yield behavior shows wide variations at different scales. The central intermediate S shows especially complex patterns of behavior in relation to the conversion of A.

Notation

c = impeller clearance
C_A^0 = initial concentration of A
C_B^f = feed concentration of B
C_I = concentration of component I
D = impeller diameter
H = liquid depth
i = radial zone position
j = axial zone position
$k_{1,2,3}$ = reaction rate constants
n = impeller rotation speed
N = network size
P_0 = power number
q = zone loop flow rate ($q = Q/N$)
Q = total internal flow rate
r_I = reaction rate
t = time
t_a = addition time
T = tank diameter
V = vessel volume
$V_{i,j}$ = volume of zone i,j

Greek letters

β = turbulent exchange flow rate
ν = kinematic viscosity

Literature Cited

Baldyga, J., and J. R. Bourne, "Simplification of Micro-Mixing Calculations: I. Derivation and Application of a New Model," *Chem. Eng. J.*, **42**, 83 (1989).

Belevi, H., J. R. Bourne, and P. Rys, "Mixing and Fast Chemical Reaction: II. Diffusion-Reaction Model for the CSTR," *Chem. Eng. Sci.*, **36**, 1649 (1981).

Bourne, J. R., F. Kozicki, U. Moergeli, and P. Rys, "Mixing and Fast Chemical Reaction: II. Model Experiments Comparison," *Chem. Eng. Sci.*, **36**, 1655 (1981).

Bourne, J. R., and S. Rohani, "Micromixing and the Selective Iodination of l-Tyrosine," *Chem. Eng. Res. Des.*, **61**, 297 (1983).

Bourne, J. R., and P. Dell'ava, "Micro and Macromixing in Stirred Tank Reactors of Different Sizes," *Chem. Eng. Res. Des.*, **65**, 180 (1987).

Bourne, J. R., and C. P. Hilber, "The Productivity of Micro-Mixing-Controlled Reactions: Effect of Feed Distribution in Stirred Tanks," *Trans. Inst. Chem. Eng.*, Part A, **68**, 51 (1990).

Brucato, A., F. Magelli, M. Nocentini, and L. Rizzuti, "An Application of the Network-of-Zones Model to Solids Suspension in Multiple Impeller Mixers," *Trans. Inst. Chem. Eng.*, Part A, **69**, 43 (1991).

Brucato, A., and L. Rizzuti, "The Application of the Networks-of-Zones Model to Solid-Liquid Suspension," *Proc. European Conf. on Mixing*, 273 (1988).

David, R., and J. Villermaux, "Interpretation of Micro-Mixing Effects on Fast Consecutive-Competing Reactions in Semi-Batch Stirred Tanks by a Simple Interaction Model," *Chem. Eng. Commun.*, **54**, 333 (1987).

Denbigh, K. G., *Chemical Reactor Theory: An Introduction*, Cambridge Univ. Press, New York, p. 111 (1966).

Drain, S., "The Development of a Competing Reaction Scheme and its Application to the Study of Mixing in Stirred Tanks," PhD Thesis, Birmingham Univ., Birmingham, U.K. (1987).

Fox, R. O., and J. Villermaux, "Micromixing Effects on the $ClO_2 + I$ Reaction: Perturbation Analysis and Numerical Simulation of the Unsteady State IEM Model," *Chem. Eng. Sci.*, **45**, 2857 (1990).

Harvey, P. S., and M. Greaves, "Turbulent Flow in an Agitated Vessel: I. A Predictive Model," *Trans Inst. Chem. Eng.*, **60**, 195 (1982).

Haywood, P. D., Associated Octel. Co. Ltd., private communication (1990).

Mann, R., and A. M. El-Hamouz, "Effect of Macromixing on a Competitive/Consecutive Reaction in a Semi-Batch Stirred Vessel," *Proc. Euro. Conf. on Mixing*, Bruges, 1 (1991).

Mann, R., and L. A. Hackett, "Fundamentals of Gas-Liquid Mixing in a Stirred Vessel: An Analysis Based on Networks-of-Zones," *Proc. Euro. Conf. Mixing*, 321 (1988).

Mann, R., and P. Knysh, "Utility of Interconnected Networks of Backmixed Zones to Represent Mixing in a Closed Stirred Vessel," *Inst. Chem. Eng. Symp. Ser.*, **89**, 127 (1984).

Mann, R., P. Knysh, E. A. Rasekoala, and M. Didari, "Mixing of a Tracer in a Closed Stirred Vessel: A Network of Zones Analysis of Mixing Curves Acquired by Fibre Optic Photometry," *Inst. Chem. Eng. Symp. Ser.*, **108**, 55 (1987).

Mann, R., P. Mavros, and J. C. Middleton, "A Structured Stochastic Flow Model for Interpreting Flow Follower Data from a Stirred Vessel," *Trans. Inst. Chem. Eng.*, **59**, 271 (1981).

Mann, R., and Y. D. Wang, "Partial Segregation in Stirred Batch Reactors: Effect of Scale-Up on the Yield of a Pair of Competing Reactions," *Trans. Inst. Chem. Eng.*, **70(A)**, 282 (1992).

Mehta, R. V., and J. M. Tarbell, "Four Environmental Model of

Mixing and Chemical Reaction: I Model Development," *AIChE J.*, **29**, 320 (1983).
Nienow, A. W., S. M. Drain, A. P. Boyes, R. Mann, A. M. El-Hamouz, and K. J. Carpenter, "A New Pair of Reactions to Characterise Imperfect Macro-Mixing and Partial Segregation in a Stirred Semi-Batch Reactor," *Chem. Eng. Sci.*, **47**, 2825 (1992).
Ng, D. Y. C., and D. W. T. Rippin, "The Effect of Incomplete Mixing on Conversion in Homogeneous Reactions," *Proc. Euro. Symp. Chem. React.*, 161 (1964).
Oldshue, J. Y., *Fluid Mixing Technology*, McGraw-Hill, New York, p. 174 (1982).
Patterson, G. K., and R. S. Brodkey, *Turbulence in Mixing Operations: Theory and Application to Mixing and Reaction*, Academic Press, New York, p. 223 (1975).
Ritchie, B. W., and A. M. Tobgy, "A Three Environment Micro-Mixing Model for a Chemical Reactor with Arbitrary Separate Feed Streams," *Chem. Eng. J.*, **17**, 173 (1979).

Manuscript received Aug. 2, 1993, and revision received May 23, 1994.